

Synthesized near field ground motion in a shallow basin

H.M. Liu¹, X. X. Tao², X. D. Sun² and P. Li²

¹ *Chongqing Communications research and Design Institute, China*

² *School of Civil Engineering, Harbin Institute of Technology, China*

Email: taoxiaxin@yahoo.com.cn taoxiaxin@yahoo.com.cn

ABSTRACT :

Near field ground motion in a shallow basin from strong earthquake occurred on a blind fault beneath is synthesized in this paper. A hybrid source model is adopted, which combines Asperity model and K square model. The ground motion at high frequency range is synthesized by a random method with dynamic corner frequency. Two steps are carried out to calculate the low frequency motion. Analytical Green Function Method is for the deeper part of the crust with source and 3D wave propagation finite element method is applied for the shallower part. The ground motion in the basin is further calculated by means of 1D equivalent linearization method at each node of calculation network. The spatial relativity of the ground motions at nodes next to each another in the basin is finally analyzed.

KEYWORDS:

near field ground motion, a shallow basin

1. INTRODUCTION

In general, the damage in urban area during earthquake is mainly from strong ground motion. The ground motion is synthesized for seismic design of structure and seismic microzonation of the city, especially for those located in a basin and near or on active faults. The near field motion is very complicated since it is governed predominantly by earthquake source. In this paper, a hybrid source model is adopted to describe the slip distribution on rupture plan. Random synthesis and numerical Green function are used to generate motions in high frequency range ($f > 1\text{Hz}$) and low frequency ($f < 1\text{Hz}$) range respectively. The input of basin effect calculation is then generated by superposition of the two motions. Seismic response of a shallow basin is calculated by means of 1D equivalent linearization procedure. As a case study, the result of the basin response from an earthquake with magnitude 6.5 is presented, and the distribution pattern of the calculated motions is summarized in the paper.

2. HYBRID SOURCE MODEL

Finite fault source model is widely adopted in simulation of near filed ground motion from large earthquake, by which the overestimation of point source model can be avoided and the rupture directivity and the hanging wall effect can be taken into account. The main idea of the hybrid source model presented herein is combining asperity model and k square model. The slip distribution on the fault plan is determined by the superposition of the slip of long wavelength calculated by asperity model and the slip of short wavelength calculated by k square model (Tao and Wang, 2004). Parameters in the model consist of three parts that are global parameters (rupture area, fault length, fault width and average slippage), local parameters (the area, location and slippage of asperity on the fault and the rupture starting point), and parameters of k square model (spatial corner wave numbers in two directions along strike and down dip) respectively. Some of them are estimated from the investigated of the fault, such as the orientation and the dip angle of the fault plan, some other parameters can be derived from a set of scaling laws (Wang and Tao, 2003) with similar form as following:

$$\log P = aM_w + b \quad (1)$$

where P is a source parameter, M_w is moment magnitude, a and b are coefficients. Figure 1 shows four examples of the source model of a given earthquake with M_w 6.5. The plan is further divided into many sub sources, and the slips are merged into each of them.

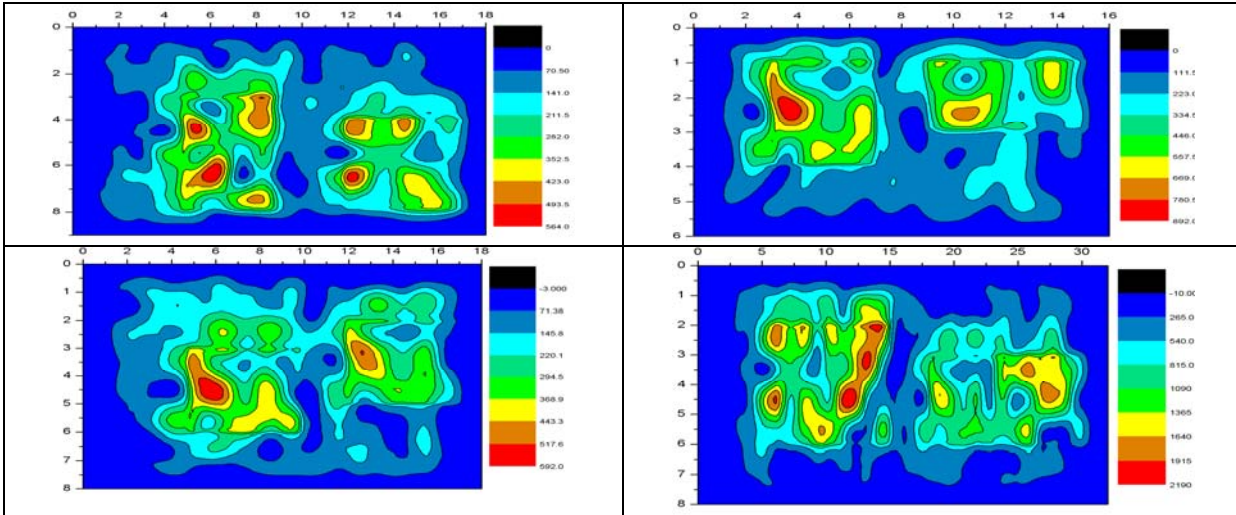


Fig. 1. Source models for an earthquake with M_w 6.5

3. SYNTHESIS OF HIGH FREQUENCY GROUND MOTION

Each sub source can be taken as a point source. Acceleration Fourier spectrum caused from a point source can be estimated from equation (2):

$$FA(M_0, f, R) = S(M_0, f) \cdot G(R) \cdot D(R, f) \cdot A(f) \cdot P(f) \quad (2)$$

where $S(M_0, f)$ is source spectrum, $G(R)$ represents geometric attenuation, $D(R, f)$ stands for inelastic attenuation, $A(f)$ is surface amplification factor, $P(f)$ is a low pass filter. The acceleration time history at a given site caused by all sub sources can be superposed in time domain with some time delays:

$$a(t) = \sum_{i=1}^{N_L} \sum_j^{N_w} a_{ij}(t - t_{ij}) \quad (3)$$

where N_L and N_w are numbers of sub sources along strike and down dip respectively, t_{ij} is the time delay of the ij th sub source from the distance between the source point to the site and the difference of the triggering time. In order to eliminate the disturbance of sub source size on high frequency radiant energy, dynamic corner frequency (Motazedian and Atkinson, 2005) is adopted herein, with which the acceleration spectrum of the ij th sub source can be described by the following form:

$$S_{ij}(M_0, f) = \frac{M_{0ij} H_{ij} (2\pi f)^2}{[1 + (f/f_{0ij})^2]} \quad (4)$$

where C is a coefficient having no dependence on frequency, M_{0ij} is the moment of the ij th sub source, H_{ij} is a compensative factor to keep the high frequency radiant energy conservation, f_{0ij} is the dynamic corner frequency which depends on the rupture area and changes as the rupture propagates.

4. CALCULATION OF LOW FREQUENCY MOTION

A two-step procedure is applied to calculate ground motions in low frequency ($f < 1\text{Hz}$) range. The whole region under consideration is divided into two parts, a deep homogenous zone with the source in it and a

shallow inhomogeneous zone from the ground surface to bottom of the upper crust. The latter is divided further into finite element network, as shown in figure 2.

Firstly, displacement time history at each node on the bottom of the overburden layer caused by each sub source is calculated by 3-order Green function as shown in equation (5).

$$F_p \times G_{np} = \sum_{i=1}^m \sum_{j=1}^n F_{\zeta} \times G_{\zeta\eta} \quad (5)$$

Displacement time histories of all sub sources at each node are superimposed to provide the input at that node in the next step. Secondly, displacement time histories at the nodes at ground surface are calculated by the space-time decoupling explicit finite element analysis with a second-order local artificial transmitting boundary (Liao et al., 1984).

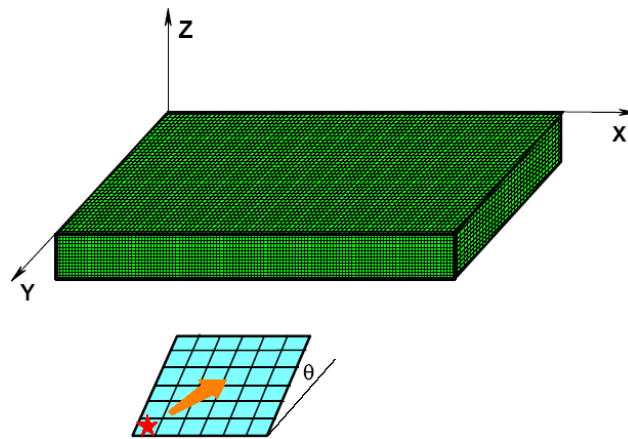


Fig. 2. Computing model for low frequency ground motion

5. SEISMIC response OF SHALLOW BASIN

The seismic response of a basin can be obtained from finite element simulation with a smaller element size for the expected frequency resolution with a detail 3-D velocity structure of the basin. It is obvious that the smaller of element size, the much more elements. For shallow basin under consideration, the total thickness of soil layers in the basin is no more than twenty meters. So the element size must be taken less than 10 meters, but which will result in unacceptable computing time and RAM space. Therefore, 1D equivalent linearization approach is adopted in the soil layer transfer function of shallow basin to describe the detail velocity structure as well as nonlinearity of soil layer.

Firstly, the basin is zoned from the thickness of soil layers. Then calculate the transfer function for each zone based on datum of boreholes in the zone. Multiply ground motions beneath the basin by the corresponding transfer function instead of the surface amplification factor $A(f)$ in Eq. (2) to get ground motion field in the basin.

Finally, the ground motions are obtained from the superimposition of high frequency ground motion and low frequency ground motion at each point in time domain after the low and high pass filtering respectively.

6. RESULT OF CASE STUDY

Figure 3 shows the PGA (peak ground acceleration) zoning map at rock site in the basin and its vicinity caused by the earthquake with magnitude 6.5 at the fault segment in the case study.

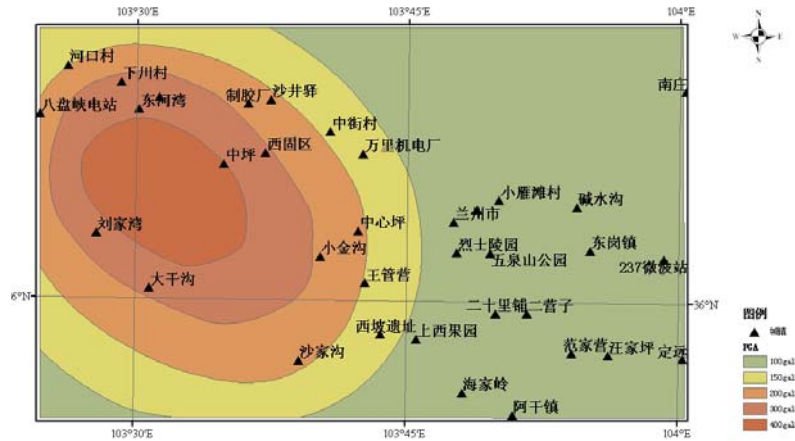


Fig. 3. Peak ground acceleration zoning map at rock site in the basin and its vicinity

Figure 4 shows the zoning map of soil condition in the basin and its vicinity. The corresponding average transfer functions of soil layer in the zones are calculated by 1D equivalent linearization approach. The surface ground motions are amplified by the soil transfer functions from those on the buried rock surface.

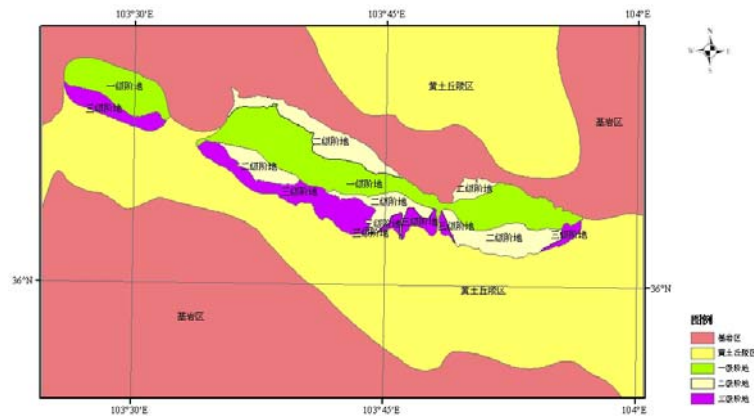


Fig. 4. Site condition zoning map in the basin and its vicinity

The peak ground acceleration zoning map is shown in figure 5. The final zoning map is presented in figure 6, in which some zones in figure 5 are divided into two or more to show the difference between the acceleration spectra with the different site conditions.

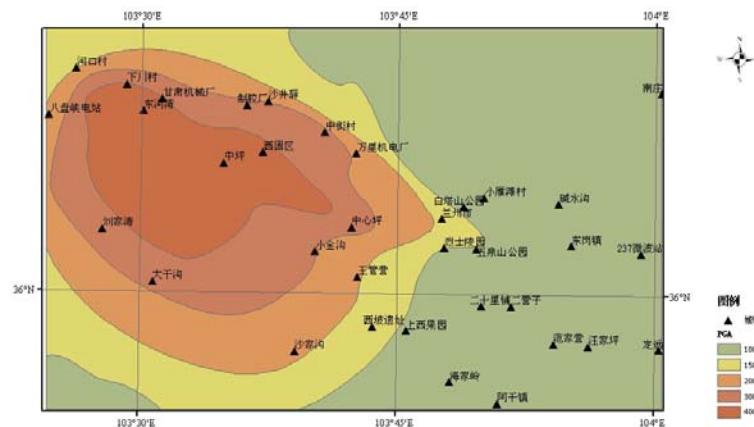


Fig. 5. PGA zoning map in the basin and its vicinity

- Atkinson G. (1984). Attenuation of strong ground motion in Canada from a random vibrations approach, *Bull. Seism. Soc. Am.*, **74**(6)
- Atkinson G. (1996). The high-frequency shape of the source spectrum for earthquakes in Eastern and Western Canada, *Bull. Seism. Soc. Am.*, **86**(1), 106-112
- Atkinson G, D.M. Boore (1997). Stochastic point-source modeling of ground motion in the Cascadia region, *Seismological Research Letter*, **68**(1), 74-85
- Atkinson G, W. Silva. 1997. An empirical study of earthquake source spectra for California earthquakes, *Bull. Seism. Soc. Am.*, **87**(1), 97-113
- Atkinson G. and D. Boore (1998). Evaluation of models for earthquake source spectra in eastern North America. *Bull. Seism. Soc. Am.*, **88**, 917-934
- Atkinson G, W. Silva, Stochastic modeling of California ground motions, *Bull. Seism. Soc. Am.*, Vol.90, No.2, 255-274, 2000
- Beresnev I. A, G. Atkinson (1999). Generic finite-fault model for ground-motion prediction in Eastern North America, *Bull. Seism. Soc. Am.*, **89**(3), 608-625
- Boore D. (1983). Stochastic simulation of high-frequency ground motions based on seismological models of the radiated spectra, *Bull. Seism. Soc. Am.*, **73**(6), 1865-1894
- Boore D. M., G. Atkinson (1987). Stochastic prediction of ground motion and spectral response parameters at hard-rock sites in Eastern North America, *Bull. Seism. Soc. Am.*, **77**(2)
- Boore D. M., W. B. Joyner (1991). Estimation of ground motion at deep-soil sites in Eastern North America, *Bull. Seism. Soc. Am.*, **81**, 2167-2185
- Boore D. (2001). Comparisons of Ground Motions from the 1999 Chi-Chi Earthquake with Empirical Predictions Largely Based on Data from California. *Bull. Seism. Soc. Am.*, **91**, 1212-1217
- Hanks T. C. (1979). B values and ω^r seismic source models: implications for tectonic stress variation along active crustal fault zones and the estimation of high-frequency strong ground motion, *J. of geophysical research.*, **84**(5)
- Hanks T.C., R.K. McGuire (1981). The character of high-frequency strong ground motion, *Bull. Seism. Soc. Am.*, **71**(6), 2071-2095
- Irikura, K. (2000). Prediction of strong motions from future earthquakes caused by active faults-case of the Osaka basin, *Proc. of 12WCEE, Auckland*